Supporting Information

Microwave-hydrothermal synthesis and characterization of nanostructured copper substituted ZnM$_2$O$_4$ (M = Al, Ga) spinels as precursors for thermally stable Cu catalysts

Synthesis details for the Cu$_x$Zn$_{1-x}$Ga$_2$O$_4$ catalyst

Gallium sulfate (Ga$_2$(SO$_4$)$_3$·xH$_2$O, Aldrich, > 99.995%), zinc sulfate (ZnSO$_4$·7H$_2$O, Fluka, > 99.5%) and cupric chloride (CuCl$_2$·2H$_2$O, Fluka, > 99%) were used without further purification and dissolved in deionized water with a metal ratio Cu:Zn:Ga of 1/8:1:2. After adjusting the pH to 10.5 with aqueous ammonia (25 % NH$_3$), the metal solution was poured into a 95 mL CEM Omni Teflon vessel and heated within 30 min to 150 °C in a MARS5 microwave reactor (CEM Corporation, 2.45 GHz, 1600 W) with five Teflon vessels per run. The constant reaction temperature of 150 °C was maintained for 1 h, followed by a cool down period of 30 min. A reference vessel equipped with an appropriate sensor was used to control the pressure and temperature during the reaction. All other vessels were temperature monitored by IR sensors. A possible overheating of the reaction inside the pressure vessel was prevented by stirring the reaction mixture and automatic power adjustment to keep the temperature constant in the range of ± 5 °C. All products were washed with deionized water, vacuum filtrated and dried in air at 80 °C for 1 h. For the catalytic MSR test twenty identical samples were assembled from the above procedure.
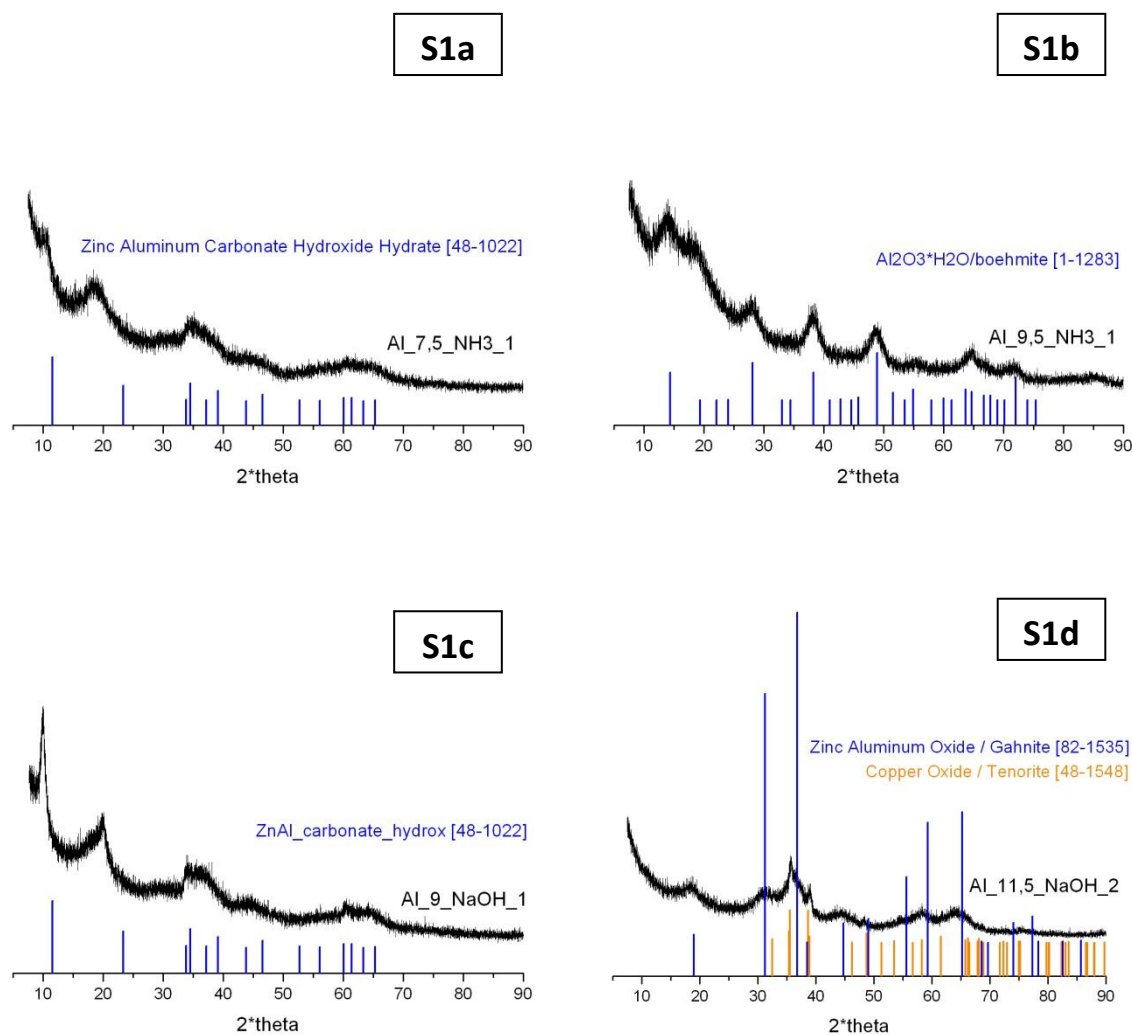
S1a

S1b

S1c

S1d

Figure S1. Representative XRD patterns of pH-dependent additional product types obtained from MW-HT treatment of a suspension of Zn-, Al- and Cu-nitrates precipitated with NH_3. 1a) initial suspension at pH 7.5 (Al_7.5_NH3_1) 1b) initial suspension at pH 9.5 (Al_9.5_NH3_1) ; precipitated with NaOH : 1c) initial suspension at pH 9 (Al_9_NaOH_1) and 1d) initial suspension at pH 11.5. In a) and c) shift of the low-angle *00l* reflections relative to those of the carbonate-hydrotalcite (blue lines) can be explained with the substitution of carbonate with nitrate anions and the expanding effect on the interlayer spacing [A. de Roy, Mol. Cryst. Liq. Cryst 311 (1998) 173-193].

Preparative and analytical notes to Figures S1 and S3: The structural difference shown in Figure S1 is furthermore reflected in the sample morphologies and compositions. SEM investigations of the hydrotalcite phases (Figure S1a,c S2a,b) showed that an unspecified microscale morphology is obtained instead of the characteristic hydrotalcite sheets. This is accompanied by an inhomogeneous distribution of copper- and zinc-rich areas (pH 7). Likewise, the boehmite products (pH > 9.5, Figure 1b) do not display distinguished morphologies (Figure S2a,c).

Further pH screening runs in the presence of NaOH brought forward a pH window between pH 9.5 and < 11 for the formation of the spinel. In line with the results for NH_3 solutions, lower initial pH values lead to hydrotalcite-related products with inhomogeneous element distributions and non-characteristic morphologies. Raising the pH to 11 and 11.5 induces the subsequent formation of CuO and ZnO impurities upon MW-HT treatment.
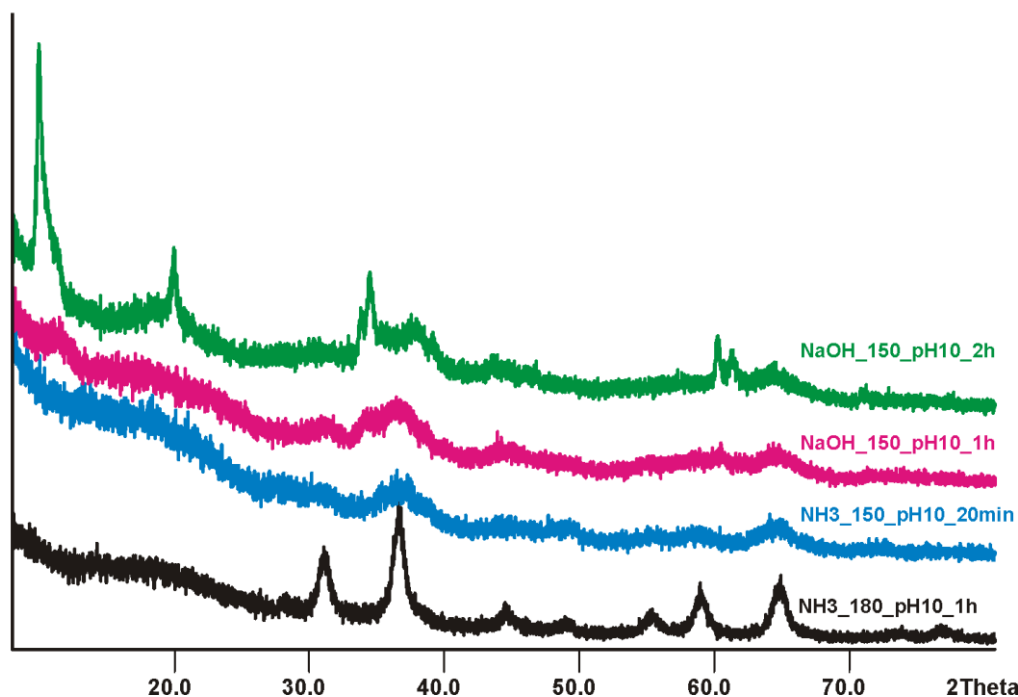
Figure S2. Parameter variation study of pristine $ZnAl_2O_4$: PXRD pattern of samples prepared all at pH 10 with NaOH (green – with only 1400 W containing hydrotalcite and 2h, pink – with 1600 W for 1h) and synthesized with NH_3 (blue – only for 20 min, black – 1h at 180 °C). Higher temperature and NH_3 as precipitating agent favor the crystallinity of the spinel material.
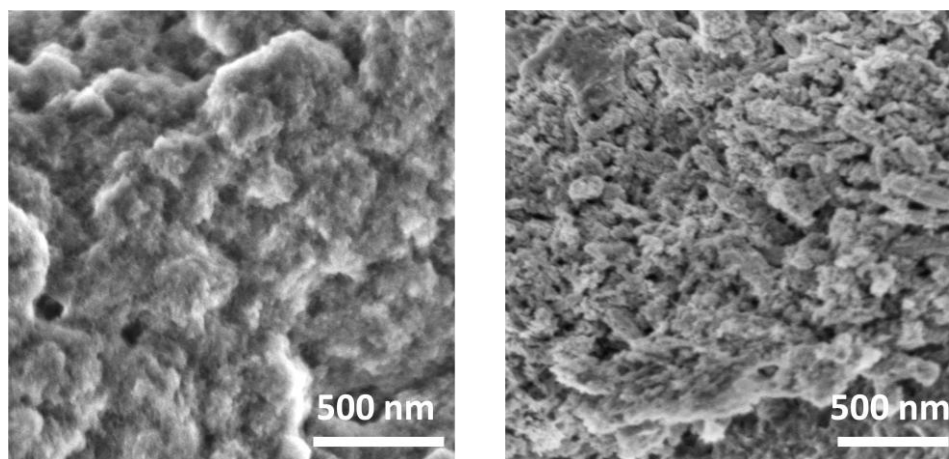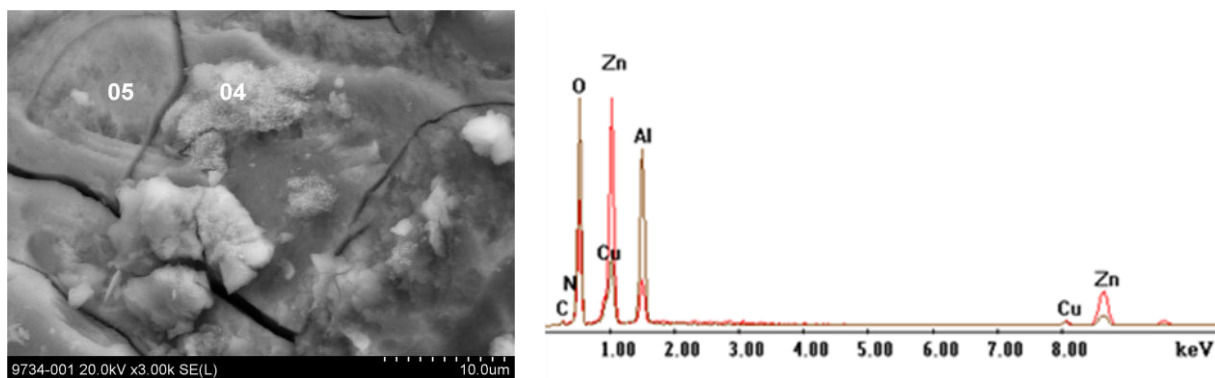

Figure S3a. Scanning electron microscopy images of $Cu_xZn_{1-x}Al_2O_4$ prepared via MW-treatment from suspensions with initial pH values of 7 (left) and 9.5 (right) with NH_3.

	spot 04		spot 05	
Element	w %	at %	w %	at %
Al	21.64	40.04	62.24	79.87
Cu	6.09	4.79	8.54	4.65
Zn	72.26	55.17	29.22	15.48

Figure S3b. Inhomogeneity of the sample Al_7_NH3_1 (hydrotalcite-containing) determined by SEM and EDX. The amount of Zn and Al varies significantly.
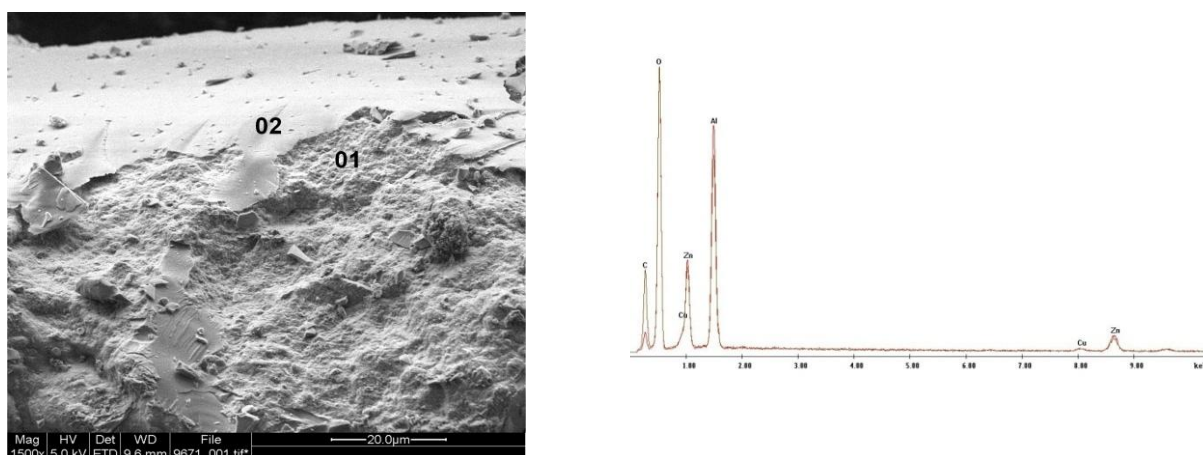

	spot 01		spot 02	
Element	w %	at %	w %	at %
Al	62.03	79.77	63.28	80.62
Cu	4.73	2.59	4.84	2.62
Zn	33.23	17.64	31.88	16.76

Figure S3c. In contrast to Figure S2b, SEM-EDX of the sample Al_9_NH3_1 (spinel) reveals a more homogenous element distribution.
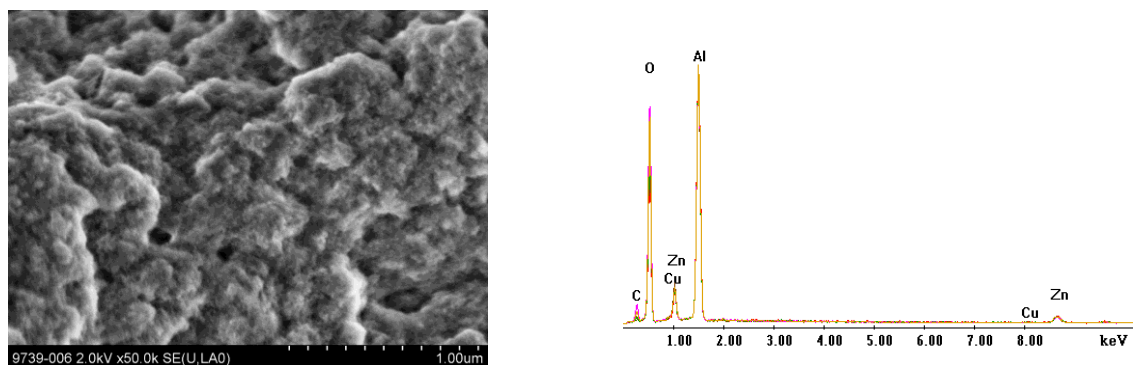
Element	spot 1 w %	spot 1 at %	spot 2 w %	spot 2 at %	spot 3 w %	spot 3 at %
Al	77.11	89.06	79.04	90.12	80.62	90.95
Cu	1.79	0.88	1.17	0.56	1.68	0.8
Zn	21.1	10.06	19.8	9.32	17.7	8.24

Figure S3d. SEM and EDX of Al_9.5_NH3_1 (spinel and boehmite) showing a relatively homogenous cation distribution, but low amounts of Cu.
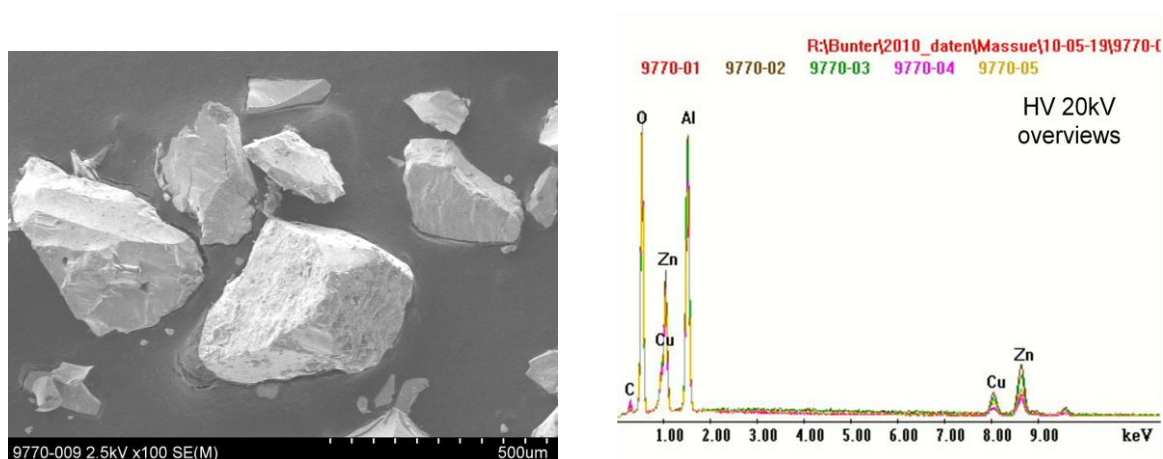
Element	w %	at %	w %	at %
Al	59.72	78.1	57.51	76.5
Cu	10.74	5.96	10.8	3.1
Zn	29.54	15.94	31.69	17.4

Figure S3e. SEM and EDX of Al_10_NaOH_1 (spinel).

Additional pH screening runs in the presence of NaOH brought forward an equally narrow but slightly more basic pH window for $Cu_xZn_{1-x}Al_2O_4$ formation that proceeds between pH 9.5 and pH< 11. In line with the above results for NH_3 solutions, lower initial pH values lead to hydrotalcite-related products with inhomogeneous element distributions and non-characteristic morphologies. Raising the pH to 11 and 11.5 induces the formation of CuO and ZnO impurities upon MW-HT treatment (Fig. S11-S13).
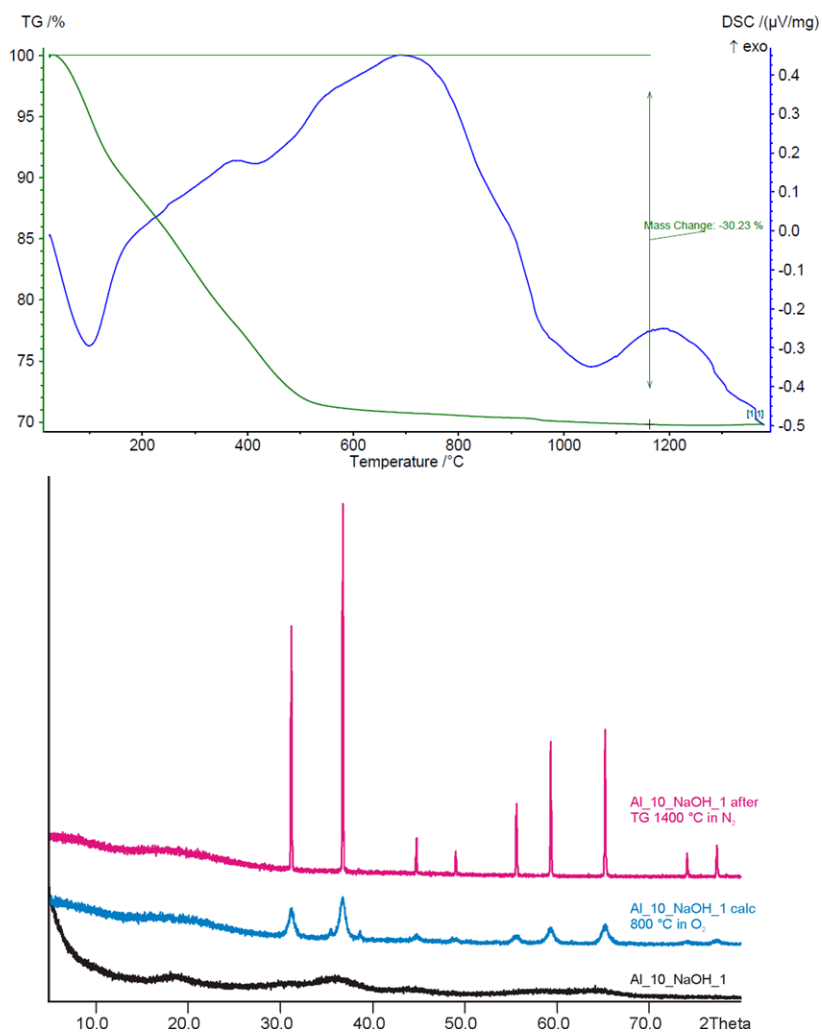
Figure S4. TG/DSC (top) and PXRD (bottom) of Al_10_NaOH_1 as prepared spinel, after calcinations at 800 °C in O_2 and after TG/DSC at 1400 °C in N_2.
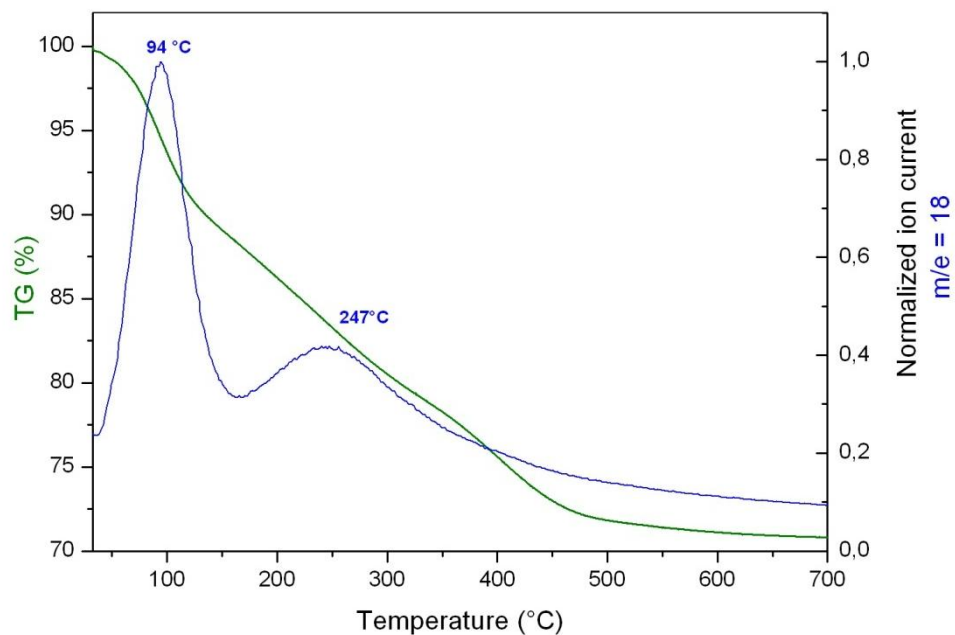
Figure S5. TG-MS of Al_10,5_NaOH_2 in synthetic air (21 % O_2 in N_2) showing at least two mass loss steps due to evolving H_2O.
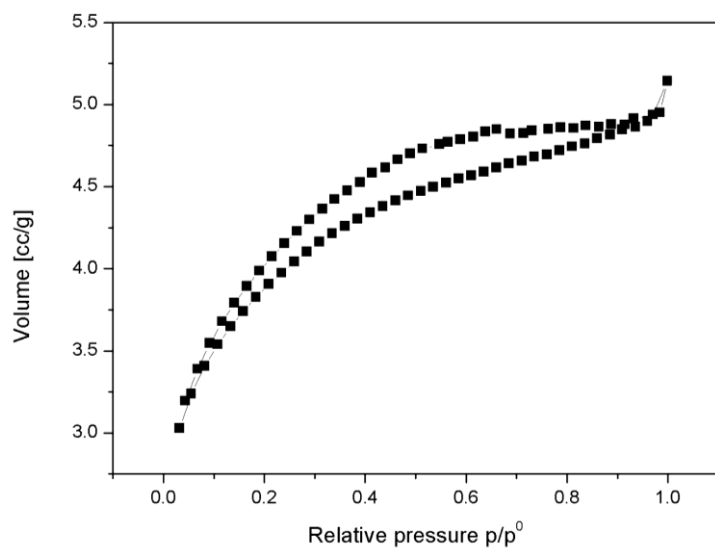

Figure S6. Nitrogen adsorption isotherm of Al_10_NaOH_2, which can be classified as a type V isotherm typical for weak interactions of adsorbent and adsorbate.
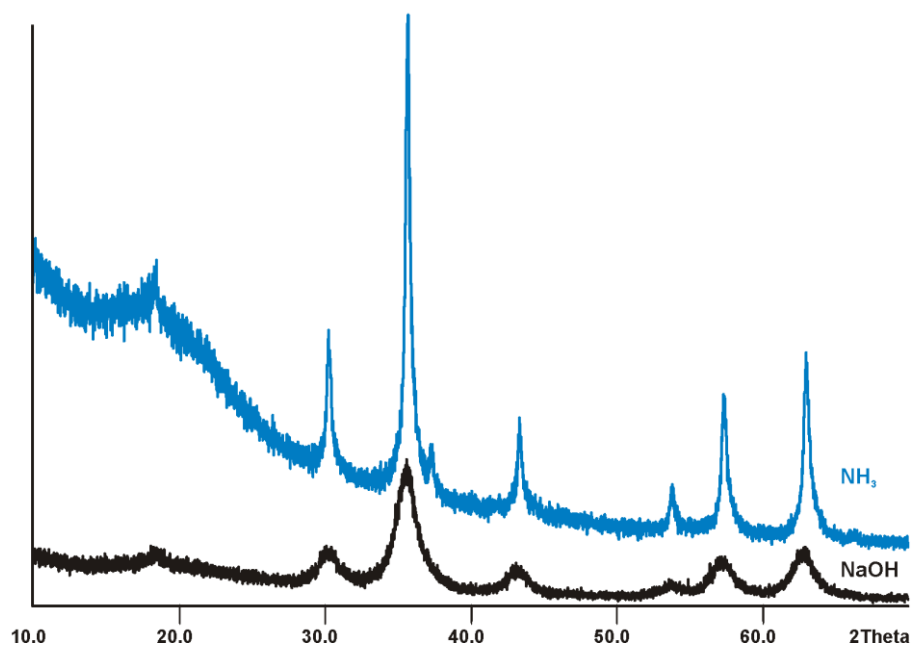
Figure S7. PXRD of ZnGa$_2$O$_4$ prepared with NaOH (blue, pH 8.1) and NH$_3$ (black, pH 10.5).

"ZnAl$_2$O$_4$"
a = 8.1090(19) Å
LVol-IB = 1.73(5) nm

Cu
a = 3.613(2) Å
LVol-IB = 1.87(14) nm

a)

"ZnAl$_2$O$_4$"
a = 8.1160(19) Å
LVol-IB = 1.706(16) nm

Cu$_2$O
a = 4.294(6) Å
LVol-IB = 4.9(4) nm

Cu
a = 3.528(6) Å
LVol-IB = 1.34(8) nm

b)

"ZnAl$_2$O$_4$"
a = 8.1152(18) Å
LVol-IB = 1.778(15) nm

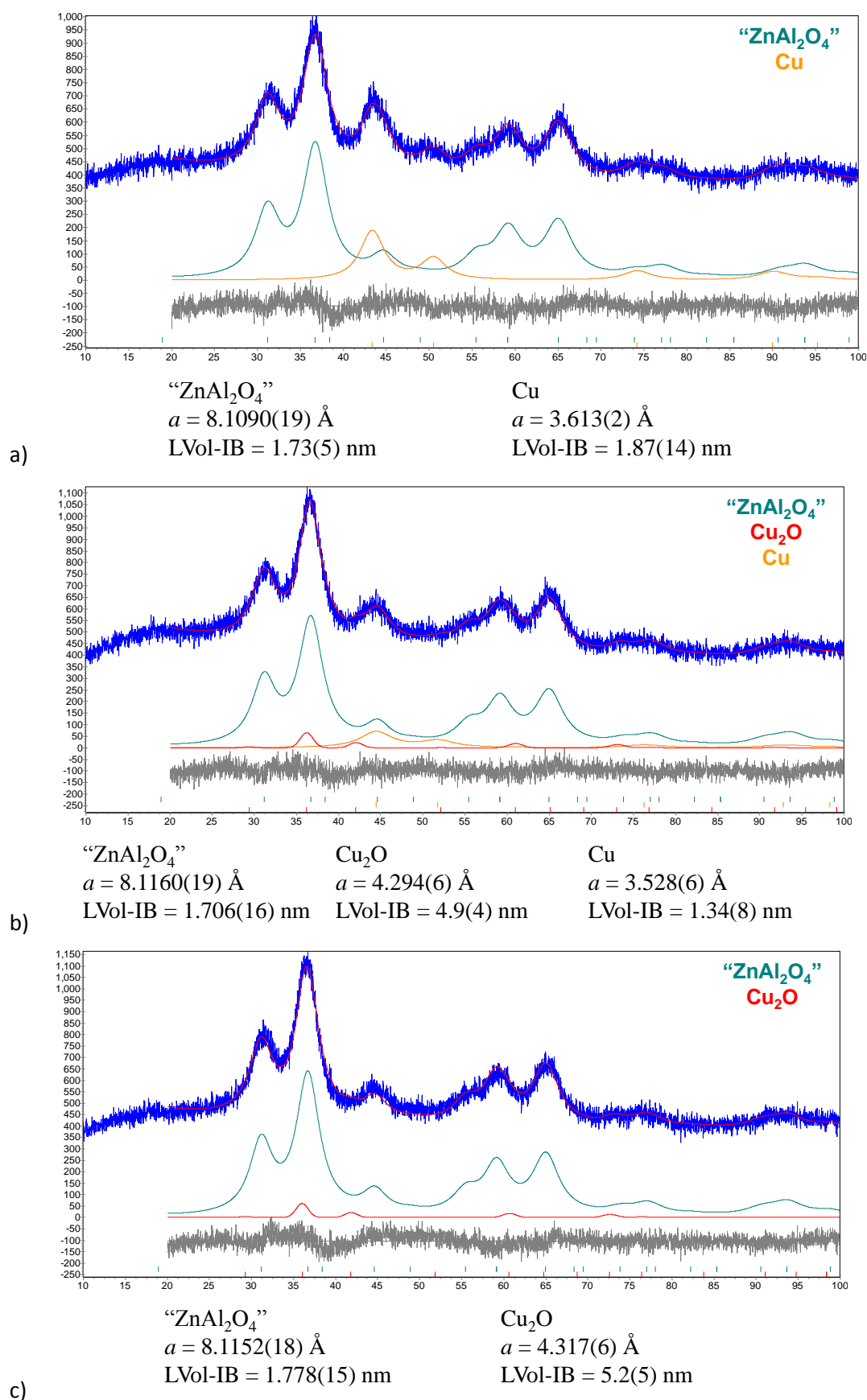Cu$_2$O
a = 4.317(6) Å
LVol-IB = 5.2(5) nm

c)

Figure S8. Rietfeld refinements of the sample Al_10_NaOH_1 after reduction at 500 °C in hydrogen (a), storage in air for 11 days (b) and re-oxidation in oxygen at 500 °C (c) using the TOPAS software package [A.A. Coelho, TOPAS Version 3.0 Bruker AXS GmbH, Germany].
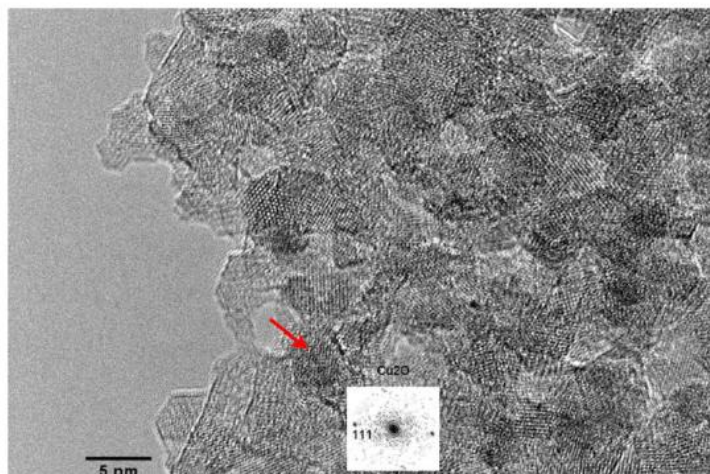
Figure S9. HRTEM-image of Al_10_NaOH_1 after reduction at 500 °C in hydrogen and subsequent re-oxidation in oxygen at 500 °C showing remaining oxidized copper particles indentified as Cu_2O (according to Fourier transform of the diffraction pattern).
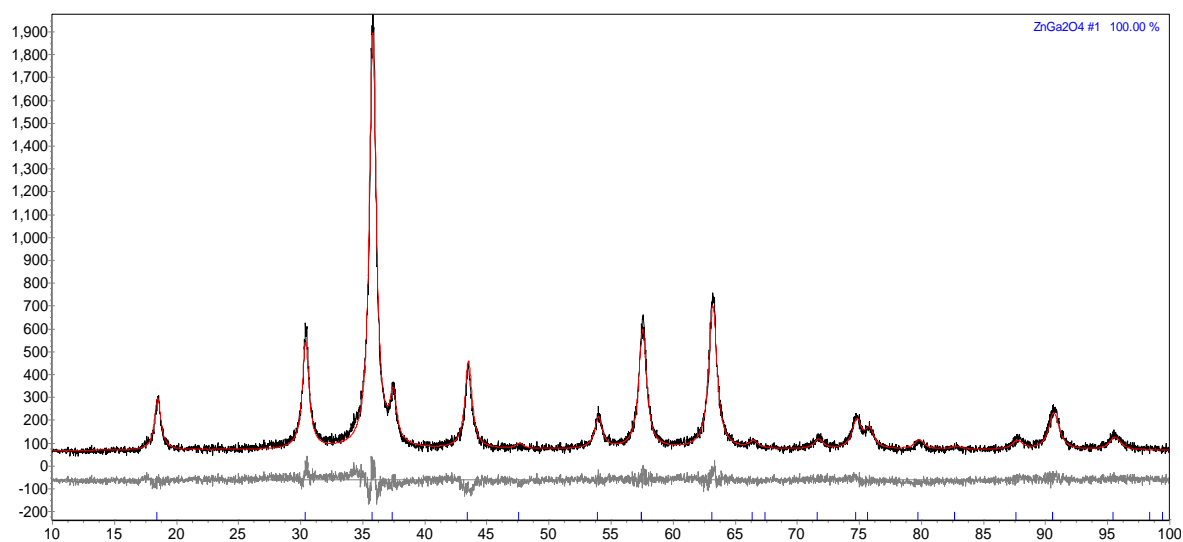

Figure S10. PXRD of Ga_10.5_NH$_3$_1after TPR at 500 °C. Formation of Cu metal is suggested by TPR (see main text), but the total amount of Cu in this sample is below the detection limit of XRD.
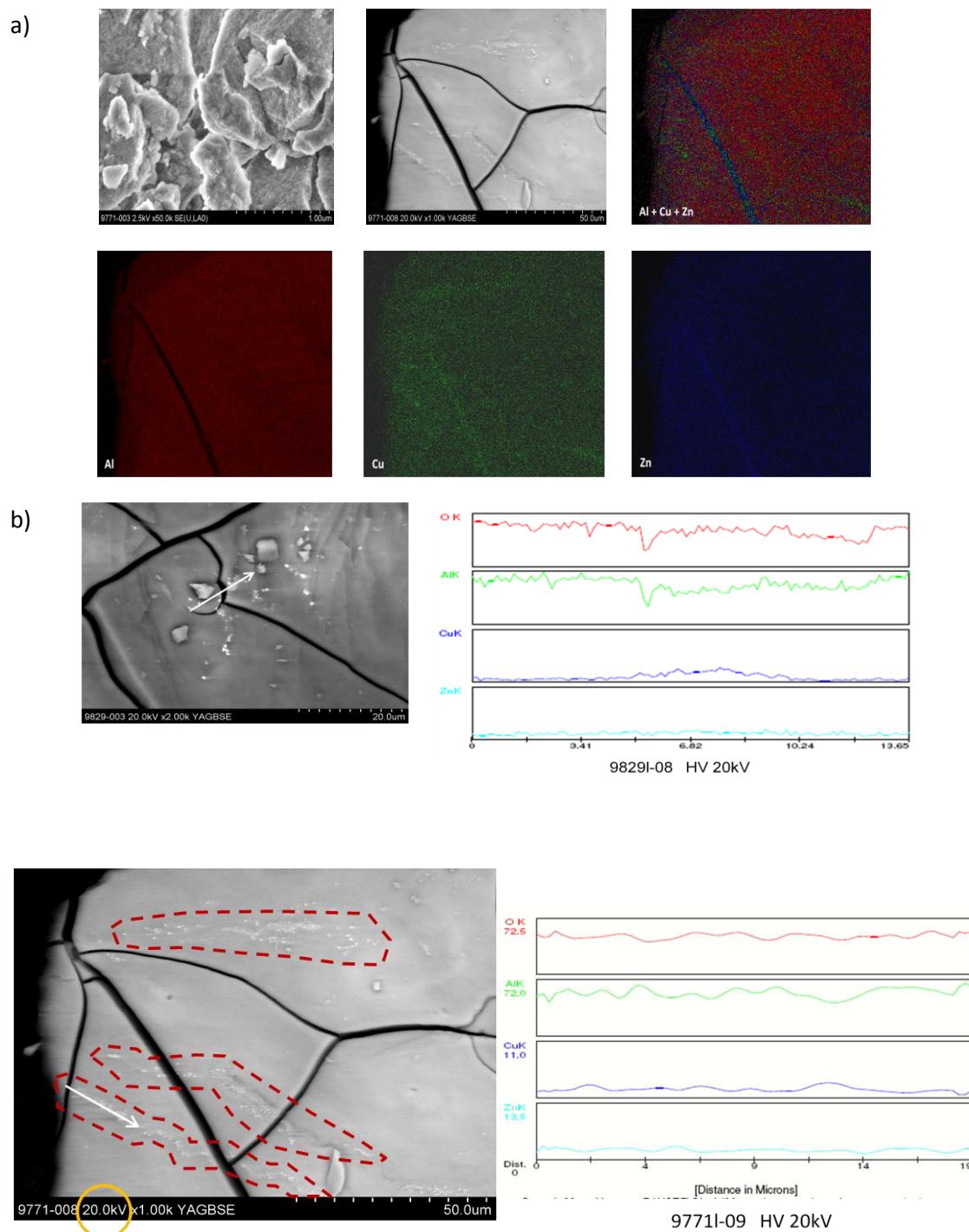
a)

b)

Figure S11. EDX mapping analyses on spinel samples obtained at pH 10 (Al_10_NaOH_2, a) and pH 10.5 (Al_10.5_NaOH_2, b) illustrate the strong pH dependence of the homogeneity of the Cu distribution (see Figure S5). At high pH, Cu-enriched particles, probably CuO, were found as segregated material appearing at bright dots in the SEM images.
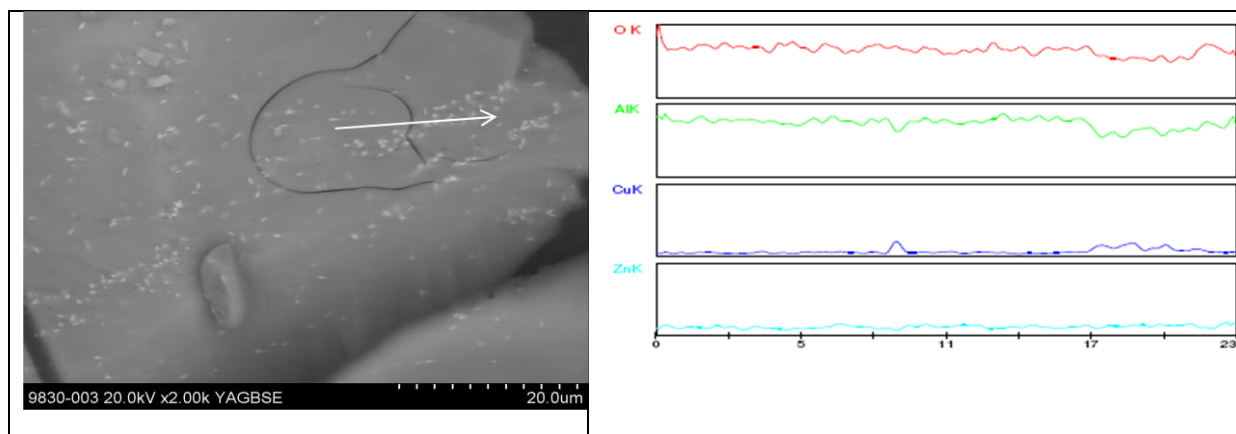
Figure S12. SEM/EDX images of Al_11_NaOH_2 indicating again the inhomogenous copper distribution in samples obtained at high pH.
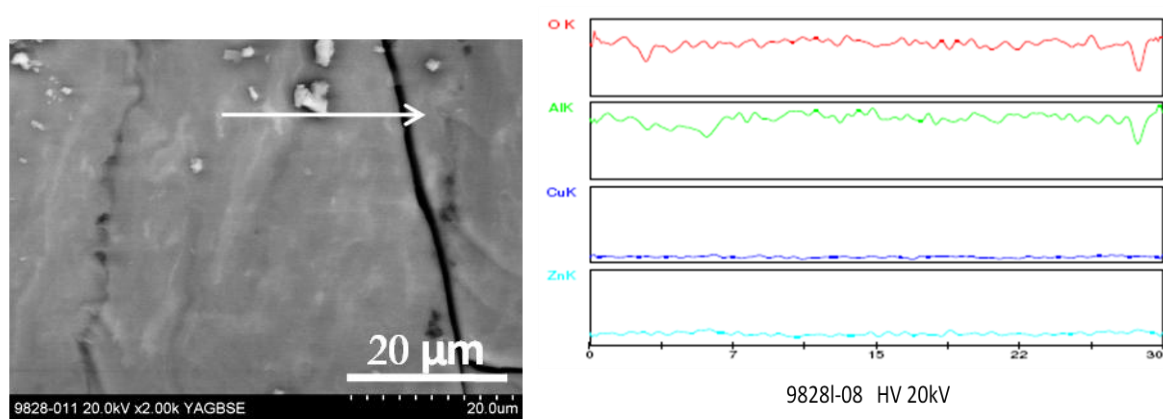

Figure S13 Similar SEM-EDX line-scan as shown in Figure S5 on a sample obtained after prolonged MW-treatment (Al_10_NaOH_2): The increased reaction time seems to diminish the amount of white CuO-like material on the surface and therefore to improve the purity and homogeneity of the sample.

Table S1. Experimental parameters of LA-ICP-MS investigations.

Parameter	Value
Laser type	ArF excimer
Laser wavelength	193 nm
Spot diameter (sample and standard)	60 μm
Repetition rate (sample and standard)	5 Hz
Laser energy	9.3 J/cm^2
He carrier gas flow rate	1.1 L min^{-1}
RF power	1350
Nebulizer gas flow rate	0.84 L min^{-1}
Auxiliary gas flow rate	0.7 L min^{-1}
Coolant gas flow rate	17.5 L min^{-1}
Dwell time	10 ms
Detector mode	Dual (pulse and analog)